Editors' Suggestion

Lone-pair-delayed persistent excitonic UV photochromism and charge transfer in Bi-doped and (Bi,Mg)-codoped stoichiometric lithium niobate single crystals

L. Kovács,* G. Corradi, Zs. Szaller, L. Bencs, G. Mandula, and K. Lengyel
Wigner Research Centre for Physics, 1121 Budapest, Konkoly-Thege Miklós út 29-33, Hungary

(Received 5 February 2024; revised 30 April 2024; accepted 13 May 2024; published 11 June 2024)

For a better understanding of the outstanding real-time photorefractive medium $LiNbO_3$:(Bi,Mg) and excitonic processes in similar systems in general, stoichiometric $LiNbO_3$ (SLN) crystals grown by two different methods and doped by Bi, Fe, or (Bi,Mg) have been investigated using low-intensity near-UV irradiation and absorption spectroscopy. Tracking down the incorporation of dopants and impurities including Fe and H by chemical and IR-UV spectroscopic analyses we assign the various spectroscopic features to specific defect complex types. Absorption bands near 4 eV overlapping the UV band edge and polarized along Nb–O bonds are ascribed to the generation of self-trapped excitons (STEs) pinned to dipolar defects consisting of Bi^{3+} or Fe^{3+} ions and their charge compensators, becoming exceptionally long-lived in the presence of lone pairs on Bi^{3+} ions. Near-UV illumination induces persistent additional absorption bands at ≈2.7 and ≈3.4 eV in Bi-single-doped crystals which can be eliminated by a short annealing above ≈150 °C or fade within a few months in the dark. These and similar photochromic bands in SLN:(Bi,Mg) are attributed to further excitations of pinned STEs, resulting in charge release. Shortening of the buildup time of the photochromic bands in (Bi,Mg)-codoped crystals is ascribed to the absence of Nb_{Li} antisite complexes serving as exciton sinks in under-threshold LN. Due to its markedly different properties an additional stable narrow band at 3.24 eV always present in SLN:(Bi,Mg) is attributed to fast reversible charge transfer processes from O^{2-} to Bi^{5+} ions on the Nb site. Processes on widely differing timescales are predicted for one- and two-photon excitations involving different excited states, relevant for further optimization of the system.

DOI: 10.1103/PhysRevB.109.214105

I. INTRODUCTION

Besides its countless nonlinear-optical applications, lithium niobate (LN) is an excellent photorefractive material used as a holographic storage medium both in the visible and near UV [1]. Slow photorefractive response, a disadvantage of LN in some applications, could be efficiently enhanced by doping engineering. Bi-doped congruent lithium niobate (CLN) crystals, especially those codoped with Mg, Zn, In, or Zr above a concentration threshold, were found damage resistant in the IR and visible (VIS) ranges, but displayed substantially improved UV photorefractive properties [2–5]. Real-time dynamic holographic displays at 442 nm have recently been demonstrated in (Bi,Mg)-codoped CLN [4,6]. The observed effects were explained by the interplay of Bi^{3+} and Bi^{5+} charge states, Bi^{5+} having a closed shell configuration and Bi^{3+} an additional lone pair in its sixth shell. Based on photorefraction and UV-VIS-IR absorption measurements [6], Bi ions displaced by the codopants from Li to Nb sites have been proposed to be responsible for the improvements. Hybrid density functional theory (DFT) calculations [7,8] confirmed the existence of Bi-related absorption bands. However, the Mg_{Li}-Mg_{Nb}-Bi_{Nb} configuration on one Li and two Nb sites suggested in Ref. [6] does not fulfill basic charge-compensation requirements.

For the interpretation of photochromic effects in LN, earlier only charge transfer processes and hopping of well-separated small-polaronic charges had been taken into account [9–12]. However, instead of separated electron-hole pairs, excitations near the UV absorption edge mostly produce localized Nb^{4+}–O^- self-trapped excitons (STEs), pinned to defects. The resulting transient absorption in this case corresponds to further excitation of these metastable states and may lead to charge separation. Joint time-resolved photoluminescence and transient absorption studies in Fe- or Mg-doped LN demonstrated the role of STEs and their long-lived pinned states [13–15]. The correct interpretation of the involved stretched exponential decay processes could only be given by a clear separation of radiative and nonradiative decay processes [14], and by taking into account flexible charge compensation by cationic defects [16].

UV-induced absorption bands surviving for minutes at RT have been noted in Mg- or Zn-doped over-threshold CLN as early as 1994 [17]. The corresponding luminescence could be quantitatively interpreted in terms of STEs pinned to Mg complexes [14]. The standard polaronic interpretation was shown to be valid only for the fast decay of other absorption bands at lower energies characterizing separated, charged small polarons. A tabular summary of various decay times observed in Fe- or Mg-doped LN together with the corresponding defect models is given in the supplemental material of Ref. [14]. UV-induced Nb^{4+}–O^- groups have been characterized by electron paramagnetic resonance in $KTa_{1-x}Nb_xO_3$

*Contact author: kovacs.laszlo@wigner.hun-ren.hu

TABLE I. Bi, Fe and (Bi,Mg)-(co-)doped SLN crystals. The first column shows the labels of the Czochralski- or HTTSSG-grown crystals used throughout the paper. The Li/Nb ratio in the boules slightly increases from top to bottom as given; its accuracy is ≈0.001.

Crystal	Li/Nb ratio in melt or solution	Li/Nb ratio in crystal top–bottom	Bi (mol %) in melt or solution	Bi (μM/M) in crystal	Mg (mol %) in melt or solution	Mg (mM/M) in crystal	Fe (mol %) in solution	Fe (μM/M) in crystal
CZ0.5	1.38	0.991–0.995	0.5	39 ± 5	–		–	7 ± 2
CZ2	1.38	0.990–0.994	2	135 ± 5	–		–	12 ± 3
CZ4	1.38	0.991–0.994	4	208 ± 4	–		–	8 ± 2
CZ2-2	1.38	N/A	2	69 ± 2	2	10.7 ± 0.8	–	1.3 ± 0.3
CZ4-1	1.38	N/A	4	145 ± 5	1	6.1 ± 0.6	–	3.1 ± 0.7
FL0.5	1	0.994–0.996	0.5	42 ± 1	–		–	8 ± 1
FL2	1	0.995–0.996	2	98 ± 2	–		–	5 ± 2
FL4	1	0.996–0.997	4	129 ± 7	–		–	1.3 ± 0.3
FL2-2	1	N/A	2	49 ± 5	2	15 ± 1	–	2 ± 1
FL4-1	1	N/A	4	200 ± 8	1	7.4 ± 0.5	–	13 ± 2
Fe0.006	1	0.996	–	N/A	–		0.006	23 ± 1
Fe0.012	1	0.996	–	N/A	–		0.012	45 ± 2
Fe0.12	1	0.996	–	N/A	–		0.12	560 ± 30

[18]. The concept of interacting STEs in LN has been recently confirmed by DFT-Bethe-Salpeter calculations of "exciton polarons" localized at lithium vacancies [19], and described also as "charge-transfer vibronic excitons" in ferroelectric oxides in general [20].

Investigating photochromic bands in the blue-near-UV range is much more feasible in stoichiometric lithium niobate (SLN) where they can be better separated from the blueshifted UV absorption edge. Along with low intrinsic defect levels, SLN also requires lower doping concentrations, ideal for defect studies and applications [21]. Photochromism and two-color holographic recording in near SLN with a Li_2O content of 49.7 mol % have been investigated in [22,23]; the observed broad UV-light-induced absorption extending from 600 nm to the UV edge could be enhanced by Tb and Fe doping and bleached by visible light. Since the observations could not be explained assuming only trapped electron polarons of shallow Nb^{4+} and deeper Fe^{2+} type, spurious electron traps with still deeper levels were suggested.

In the present work our goal is to explore photochromic effects in Bi- or (Bi,Mg)-doped SLN crystals and to propose improved models and assignations for the underlying defects and processes characterizing also the polarization and temporal behavior of photoinduced phenomena. The effect of exchange-coupled lone pairs stabilizing the Bi^{3+} charge state in subgap excitations is elucidated by a systematical separation of STE and charged-polaron related effects, supported by comparisons with previous and recent data on Fe-doped SLN.

II. EXPERIMENT

Two sets of SLN crystals have been grown by the Czochralski and the high-temperature top-seeded solution growth (HTTSSG) [21] methods, respectively, using high-purity Starck LN grade Nb_2O_5 and Sigma-Aldrich 4N Li_2CO_3 raw materials. For Czochralski-grown crystals the Li/Nb ratio in the melt was 1.38. For single-doped samples the amount of Bi added to the melt as high-purity Bi_2O_3 was 0.5, 2, or 4 mol %. Double-doped crystals were also grown, either with 2 mol % Bi and 2 mol % Mg, or 4 mol % Bi and 1 mol % Mg. Boules of ≈15 mm diameter and 20–30 mm length were grown along the ferroelectric *c* axis with pulling and rotation rates of 0.5–0.8 mm/h and 3.5–6 min^{-1}, respectively. An analogous series of SLN crystals has been prepared by HTTSSG with K_2O flux, Li/Nb = 1, and pulling and rotation rates of 0.12–0.15 mm/h and 44–46 min^{-1}, respectively. Table I summarizes the crystals used including Fe-doped SLN grown by HTTSSG for comparison. The Czochralski-grown crystals are shown in Fig. 1. Despite some small cracks for high dopant concentrations, crack-free, oriented samples could be prepared from all boules. *Z* cuts from the top and bottom parts with a thickness of 1 or 4 mm were polished for UV-visible and IR absorption studies, respectively, together with some *Y* cuts (1 mm) for polarized measurements. Fourier-transform infrared absorption spectroscopy has been used to determine the crystal stoichiometry using a Bruker IFS 66v/S spectrometer with a resolution of 0.2 cm^{-1}.

The amounts of dopant elements (Bi, Fe, Mg) incorporated into the crystals have been determined by flame and graphite furnace atomic absorption spectrometry, using a ContrAA-700 instrument (Analytik Jena AG, Jena, Germany). The chemical analyses of the doped and undoped SLN crystals were performed after dissolution of the powdered samples (Bi, Fe) or with solid sampling (Mg) as described in detail in Refs. [24,25]. The effective distribution coefficient of Bi, calculated from the data presented in Table I, was found to

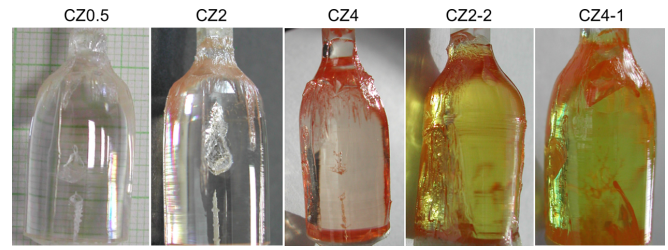

FIG. 1. Bi-doped and (Bi,Mg)-codoped Czochralski-grown SLN crystals. See a millimeter-grid graph paper in the background, and Table I for labels.

be extremely low, ≈(2–8) × 10^{-3}, decreasing with improved stoichiometry and an order of magnitude lower than the value of ≈ 4 × 10^{-2} reported earlier for crystals far from stoichiometric [26]. The reasons for the small distribution coefficient can be the larger ionic radius of Bi compared to Li or Nb [27], the scarcity of charge-compensating intrinsic defects with improving stoichiometry, and lone-pair effects to be discussed later. As a cross check, we measured the Bi content of the crucible residue by energy dispersive x-ray spectroscopy (EDAX), and found it to be somewhat higher than expected. However, the built-in Bi concentration significantly exceeded the background Fe concentration (Table I).

Optical absorption has been measured from RT to 250 °C by a Cary 4000 spectrophotometer in the 300–900 nm range with a resolution of 1 nm. A UV lamp with total intensity of ≈0.4 mW/cm^2 peaking at ≈3.4 eV was used for sample illumination before measurements. Luminescence measurements were attempted at RT using a Jobin Yvon Fluorolog 221 spectrofluorometer with a Xe lamp, but no characteristic emission could be detected.

III. EXPERIMENTAL RESULTS

A. IR absorption spectra

In SLN:Bi where the built-in Bi concentration was low compared to that of intrinsic defects, the absorption bands of hydroxyl ions could be used to determine the Li/Nb ratio [28]. For double-doped crystals no such calibration is available. A composition closer to stoichiometric was found in the bottom part of the boules. Taking into account the thermal and temporal history of the samples [28], Li/Nb ratios in the 0.990–0.997 range were found for all single-doped crystals (Table I), corresponding to a Li_2O content of 49.8–49.9 mol %. The composition in HTTSSG crystals was more homogeneous and slightly closer to stoichiometric compared to Czochralski-grown crystals. The Fe-doped crystals grown from flux showed under-threshold behavior with Li/Nb ≈ 0.996.

In SLN:(Bi,Mg) crystals the frequency of the main OH^- vibration is shifted to 3535 cm^{-1} (Fig. 2) characteristic for over-threshold crystals (the threshold Mg concentration is ≈5 mol % in CLN and less than 1 mol % in SLN [29]). In addition to the 3535 cm^{-1} band with its typical shoulder at ≈ 3525 cm^{-1}, in codoped crystals a weak band appeared at 3492 cm^{-1}. This can be attributed to the stretching vibration of the OH^- ion in a $Bi_{Nb}^{3+} - OH^-$ complex ($Bi_{Nb}^{2-} - OH_O^+$ in the Kröger-Vink-type notation displaying charges relative to the perfect lattice, to be used in the following) similarly to the case of other trivalent-ion-doped SLN crystals or those additionally doped with Mg, discussed in Ref. [30]. No such band was detected in Bi-single-doped crystals, indicating that Bi ions only occupy Li sites, while in double-doped crystals Bi at least partly substitutes for Nb. One can estimate the amount of hydroxyl ions from the integrated area under the OH^- bands using calibrations for oxide crystals, specifying an integrated absorption of 1 × 10^{-17} cm^{-2} for 1 OH^- ion/cm^3 [31]. Accordingly, the areas ≈0.4 and ≈20 cm^{-2} of the bands at 3492 and 3535 cm^{-1} in sample CZ2-2 correspond to ≈2 × 10^{-6} and 1 × 10^{-4} M/M of $Bi_{Nb}^{2-} - OH_O^+$ and $Mg_{Nb}^{3-} - OH_O^+$ complexes, respectively. Both OH^- concentrations are more than an order of magnitude lower than the actual built-in dopant concentrations, meaning that only a small part of the dopants is associated to OH^-.

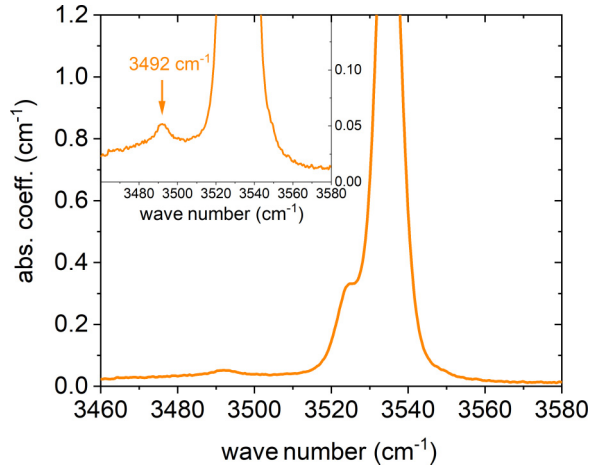

FIG. 2. OH^- absorption spectrum of (Bi,Mg)-codoped SLN, sample CZ2-2. The inset shows a band at 3492 cm^{-1} attributed to O-H vibration in a $Bi_{Nb}^{2-} - OH_O^+$ complex.

B. UV-VIS absorption spectra

As seen in Fig. 1, all Bi-doped crystals turned reddish brown with growing Bi content, but with a yellowish tinge for double-doped crystals. Moreover, the crystals became more and more reddish brown with increasing time of exposure to natural light (see Sec. III C). This coloration could be eliminated by a short annealing at $T \geqslant 250$ °C. Figures 3(a) and 3(b) show the absorption spectra of Bi-single-doped SLN crystals subjected to a 1 h annealing at 500 °C and stored in the dark to restore the "as-grown" state, together with those of undoped and Fe-doped SLN for comparison. No absorption near a closely exponential UV edge is observed in our "best Fe-free" undoped SLN samples [21] proving that the near-UV bands seen in doped samples are of extrinsic character.

The spectra of Czochralski- and flux-grown crystals shown in Figs. 3(a) and 3(b), respectively, have similar shapes for Bi- and Fe-doped crystals. For both dopants, the absorption maxima increase linearly with the respective built-in concentration [Fig. 4(a)]. Although the slope of the fit is the highest for Fe-doped crystals, in Bi-doped crystals the background Fe concentration of the order of only 10 μM/M cannot be responsible for the substantial near-UV absorption observed. The different slopes of the linear fits in Figs. 4(a) and 4(b) indicate that, apart from a possibly larger absorption cross section of the transition in the Fe case, in flux-grown crystals a much smaller fraction of Bi defects is participating in the absorption than in Czochralski-grown ones.

Gaussian fits of the absorption increment due to Bi doping show a single absorption band at ≈4.0 eV with a half width at half maximum (HWHM) of ≈0.36 eV [see Fig. 3(d) and Table II]. Similar values have been obtained from Gaussian fits in Fe-doped crystals [Fig. 3(e) and Table II] indicating a similar origin of the near-UV absorption band in both crystals. Controlling Fe impurities in Bi-doped samples is crucial for

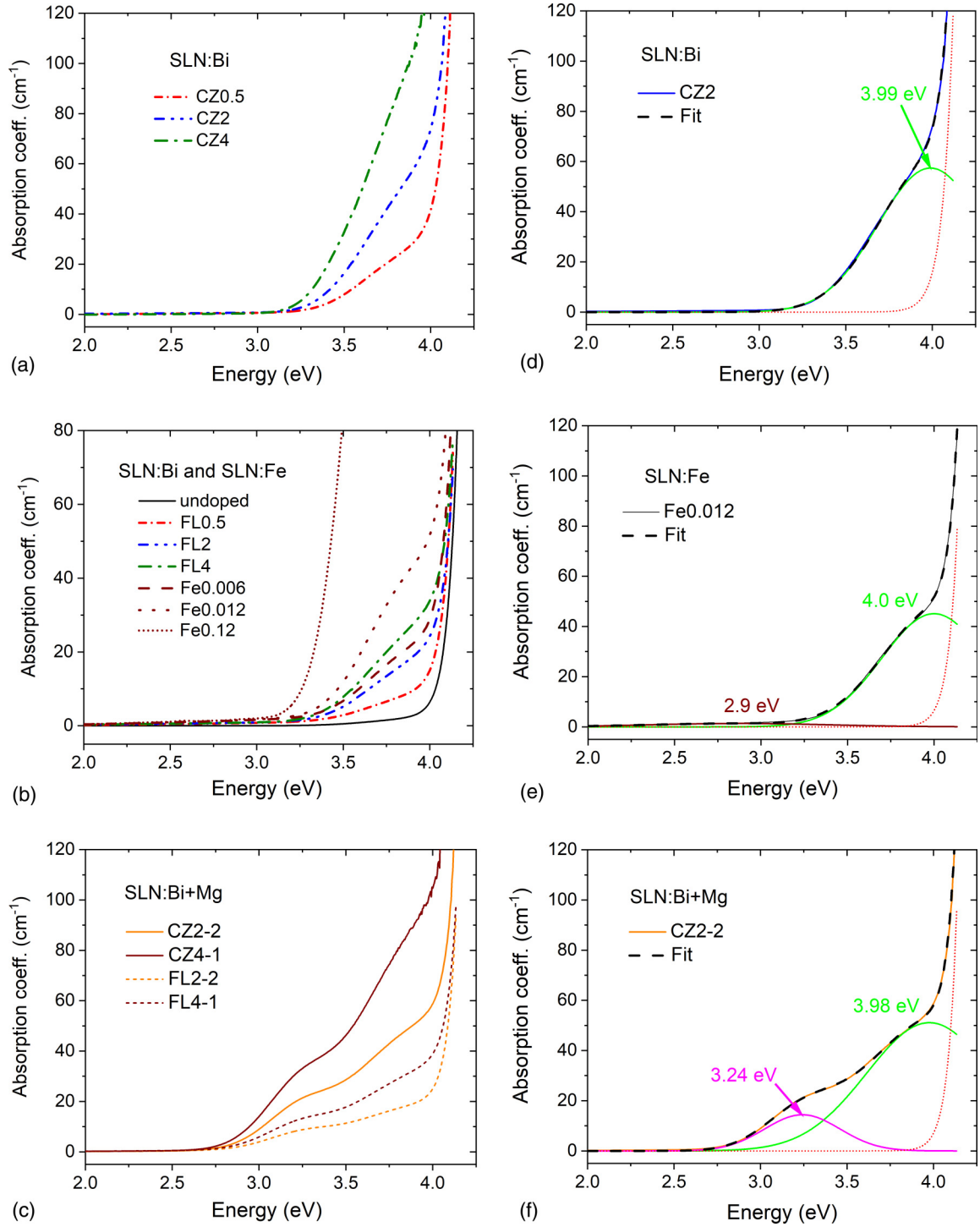

FIG. 3. Unpolarized UV-VIS spectra of Bi-doped (a), (b) and (Bi,Mg)-codoped (c) samples annealed and stored in the dark compared with those of as-grown undoped and Fe-doped (b) crystals. For sample codes see Table I. Fits using Gaussian dopant-induced bands and an exponential Urbach edge (red line) provide almost undistinguishable reproductions (dashed lines) of the spectra (d)–(f). The small band near 2.9 eV in part (e) remains unidentified and may be influenced by the presence of a small number of stable Fe^{2+} small polarons.

a clear separation of the effect caused by Bi. In fact, the observed near-UV absorption band in SLN:Fe [Figs. 3(b) and 4(a)] clearly corresponds to the "iron *C* band" described in CLN [32,33] where its maximum could not be pinpointed due to overlap with the redshifted UV edge (see also Sec. IV C).

The distinctive yellowish tinge of (Bi,Mg)-codoped crystals (Fig. 1) can be seen to originate from an absorption band around 3.24 eV with a HWHM of ≈0.26 eV [Figs. 3(c) and 3(f)]. Similar but much broader spectra have been observed in CLN:(Bi,Mg) [6]. The other component around 4.0 eV, determined from the Gaussian fit [Fig. 3(f)], looks similar to that seen in SLN:Bi, apart from slight broadening. For both components, the intensities are again markedly lower in the case of flux-grown crystals.

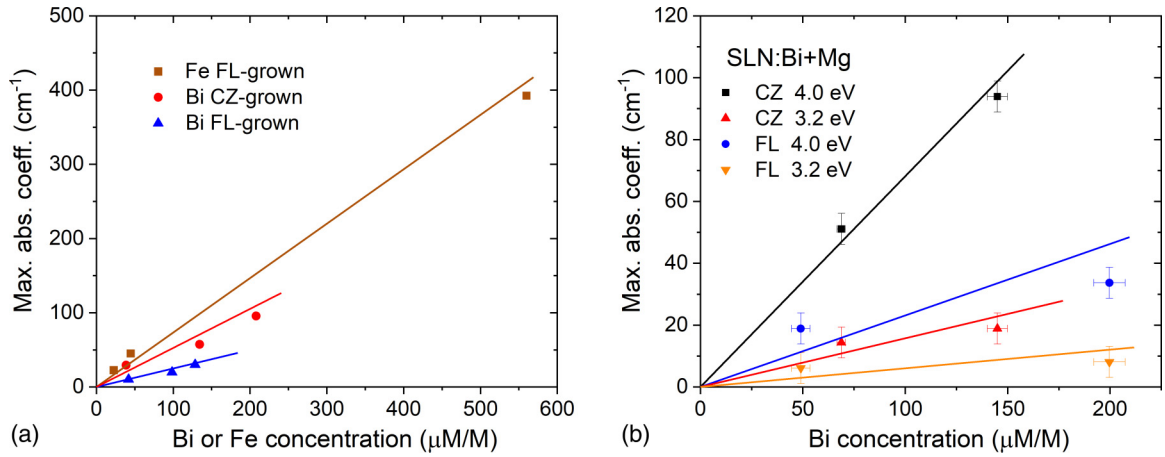

FIG. 4. Dependence of the maximum absorption coefficients of the fitted component bands for unpolarized light in Bi- or Fe-doped (a) and (Bi,Mg)-codoped (b) as-grown crystals on the built-in dopant concentration.

The absorption spectra of Fe-, Bi-, or (Bi,Mg)-doped crystals have also been measured in *Y*-cut samples using polarized light. The amplitude of the ≈4.0 eV band for ordinary $\underline{E}\perp c$ polarization in all cases strongly exceeded that for parallel polarization (Fig. 5). The 3.24 eV band in (Bi,Mg)-codoped crystals showed an opposite behavior. The angle θ between the direction of the electrical dipole moment of the transition and the Z$\|c$ axis could be calculated from the formula $\tan^2\theta \approx A_X/A_Z$, where A_X and A_Z are the extremal absorbance values for $\underline{E}\perp c$ and $\underline{E}\|c$, respectively [31]. The obtained values of θ are shown in Table II.

C. Photochromic effect in Bi and (Bi,Mg)-codoped SLN crystals

Intense darkening with increasing time of exposure to natural light or UV irradiation has been observed in all Bi-containing crystals, in contrast to undoped and Fe-doped ones. The UV-induced photochromic change between 2 and 4 eV in annealed SLN:Bi is shown in Fig. 6(a). A Gaussian fit revealed two components at 2.74 and 3.41 eV with HWHMs of 0.45 and 0.37 eV, respectively. The ratio of the integral intensities of the components remained close to 1 during irradiation. The effect saturated in ≈30 min (see end of section) and showed no essential changes during dark storage for several weeks, but eventually disappeared after storage for

TABLE II. Absorption bands and their parameters in Mg-, Bi-, or Fe-doped, and (Bi,Mg)-codoped CLN and SLN crystals. The experimental error was ±0.05 eV for our measured *M* and *W* values, and ±2° for the polar angle θ of the transition dipole.

Crystal	CLN:Mg	CLN:Bi	CLN:(Bi,Mg)	CLN:Fe	SLN:Bi	SLN:(Bi,Mg)	SLN:Fe
Mol % added	5% - 6.5%	0.5%→1.5%	0.5%→1.5% +5.5%→6.5%	0.1%	2%	2% + 2%	0.012%
Sample code					CZ2	CZ2-2	Fe0.012
As-grown bands							
Band max *M* (eV)	4.03[a]	3.65→3.53	3.15→3.35	>3.1	3.99	3.24 3.98	4.00
HWHM=*W* (eV)	0.28[a]				0.36	0.26 0.43	0.36
W^2/M (eV)	0.02[a]				0.032	0.020 0.046	0.032
Dipolar angle θ					54°	36° 53°	53°
Near-UV-induced bands							
Band max *M* (eV)	2.64 3.45			≈2.9[b]	2.74 3.41	2.92 3.67	No stable bands at RT
HWHM *W* (eV)	0.63 0.37			0.5[b]	0.45 0.37	0.43 0.29	
W^2/M (eV)	0.15 0.04			0.086[b]	0.074 0.040	0.063 0.023	
Buildup time $\tau_{buildup}$	70 ms[c]			≈5 μs[c]	≈141 s[d]	≈8 s[d]	
$\beta_{buildup}$	0.8[c]			≈0.39[c]	0.8[d]	0.6[d]	
Decay time τ_{decay}	13 s 112 s 10 s[c]			≈4 s[c]	Months	Months	
β_{decay}	0.68 0.72 0.45[c]			≈0.61[c]			
Decay temp.					≈ 150 °C	≈ 200 °C	
References	[11,13]	[2]	[6]	[15,13]	This work	This work	This work

[a]Measured at $T = 3.8$ K in CLN:Mg(5%) [11].
[b]$E_{exc} = 3.45$ eV pulse-induced transient spectrum in CLN:Fe(0.1%) [15].
[c]Two-photon pulse-induced transient probed at 445 nm (2.79 eV) in CLN:Mg(6.5%) or CLN:Fe(0.1%) [13].
[d]UV lamp with total intensity of 0.4 mW/cm^2.

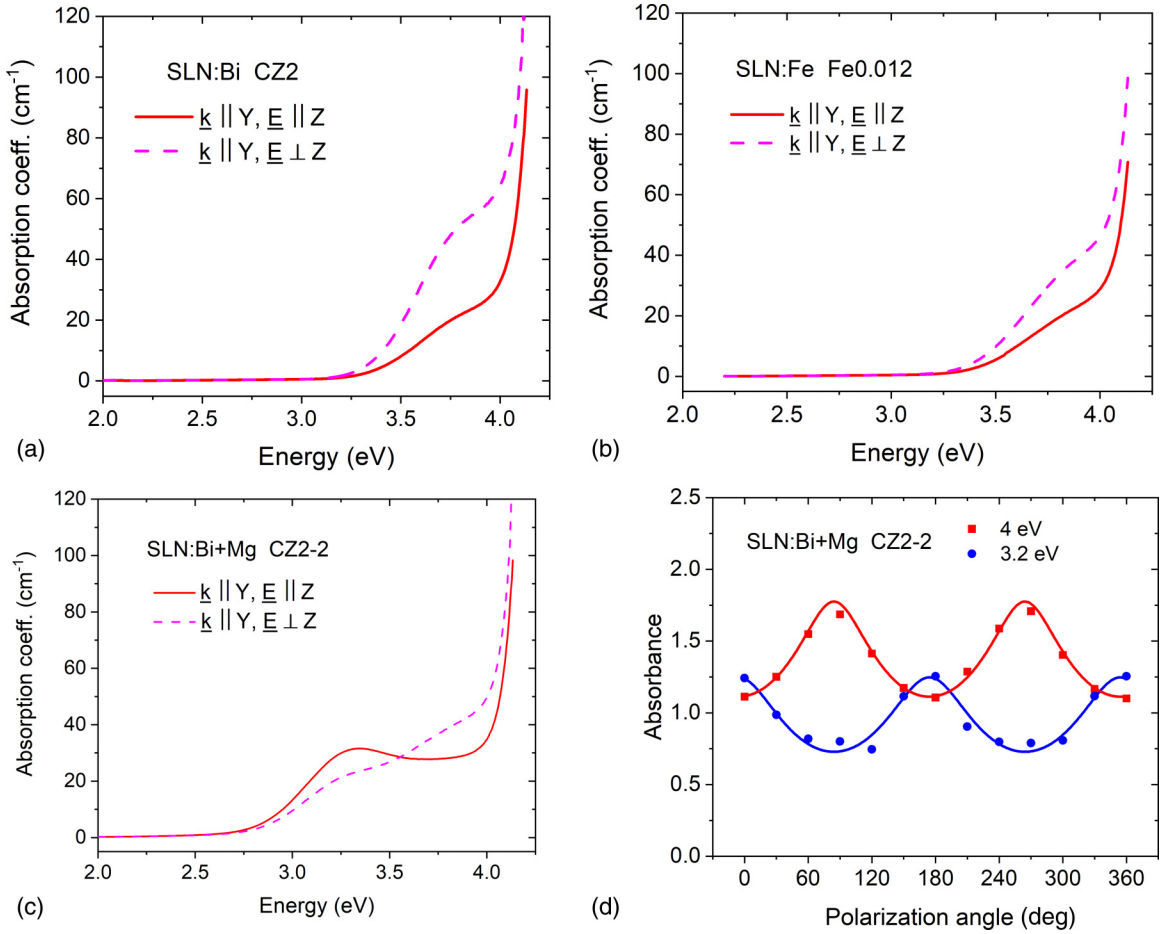

FIG. 5. UV-absorption spectra of as-grown SLN Bi-doped (a), Fe-doped (b), and (Bi,Mg)-codoped (c) for polarization parallel and perpendicular to the $Z\|c$ axis. Polarization dependence of the 4.0 and 3.2 eV band maxima in SLN:(Bi,Mg) (d). Values of the polar angle θ of the transition dipole moment are calculated from the fitted curves (see text and Table II).

1 year and thus proved to be persistent at RT for months. Upon heating the components disappeared in the 100 °C–180 °C temperature range (see Fig. 7, blue quadrangles).

A similar photochromic effect has been observed in SLN:(Bi,Mg) as shown in Fig. 6(d) for sample CZ2-2. The photochromic absorption, slightly blueshifted compared to SLN:Bi, could again be fitted by Gaussians at ≈2.92 and ≈3.67 eV with HWHMs of 0.43 and 0.29 eV, respectively [Fig. 6(e)], with an integral intensity ratio $I_1/I_2 \approx 2.5$ essentially unchanged during illumination. No photoinduced change of the as-grown bands themselves near 3.2 and 4.0 eV could be found. The near-UV-induced bands also showed some preference for ordinary polarization, both for single and double doping, like the ≈4.0 eV as-grown bands. However, taking into account the relatively weak photoinduced absorption, 1%–5% compared to the absorption of the as-grown samples, only a crude estimate $\theta \geqslant 45°$ for the polar angle of the transition moment could be deduced.

The photochromic saturation was found to occur much faster in double-doped than in Bi-single-doped SLN [Figs. 6(c) and 6(f)]. The time constant τ_{buildup} determined by fitting a stretched exponential to the photochromic absorption change at its maximum was more than a magnitude shorter in SLN:(Bi,Mg) (≈8 s), than in SLN:Bi (≈141 s). The corresponding stretching factors β (see Ref. [14]) were 0.8 and 0.6, respectively. These parameters, in particular τ_{buildup}, are expected to depend strongly on the parameters of the excitation source. Thermal annealing treatments of the near-UV-induced absorption in SLN:(Bi,Mg) revealed higher decay temperatures of 160 °C–250 °C compared to SLN:Bi for both component bands without clear differences between them (Fig. 7, red dots). Finally, it should be noted that no persistent photoinduced change could be observed in SLN:Fe.

IV. DISCUSSION

A. Incorporation of Bi

Compared to Nb, Bi has a clear preference for the +3 oxidation number as described by its higher electronegativity. Its monoclinic Bi_2O_3 oxides [34,35], only contain strongly distorted Bi^{3+} sites, while the less stable mixed-oxide Bi_2O_4 [36], prepared using daylong hydrothermal reactions at $T \leqslant 200$ °C in the presence of alkaline nitrates, has also nearly regular octahedral Bi^{5+} sites. Along with unstable Bi_2O_5 [34], several reduced-stability double oxides with hexagonally close-packed oxygen sublattices comparable to LN, but containing Bi^{5+} instead of Nb^{5+}, have also been prepared, including orthogonal $LiBiO_3$ [37], ilmenite-type $NaBiO_3$ and $AgBiO_3$, and also trirutile-type $MgBi_2O_6$ ([38] and references therein). Above ≈ 300 °C these compounds begin losing

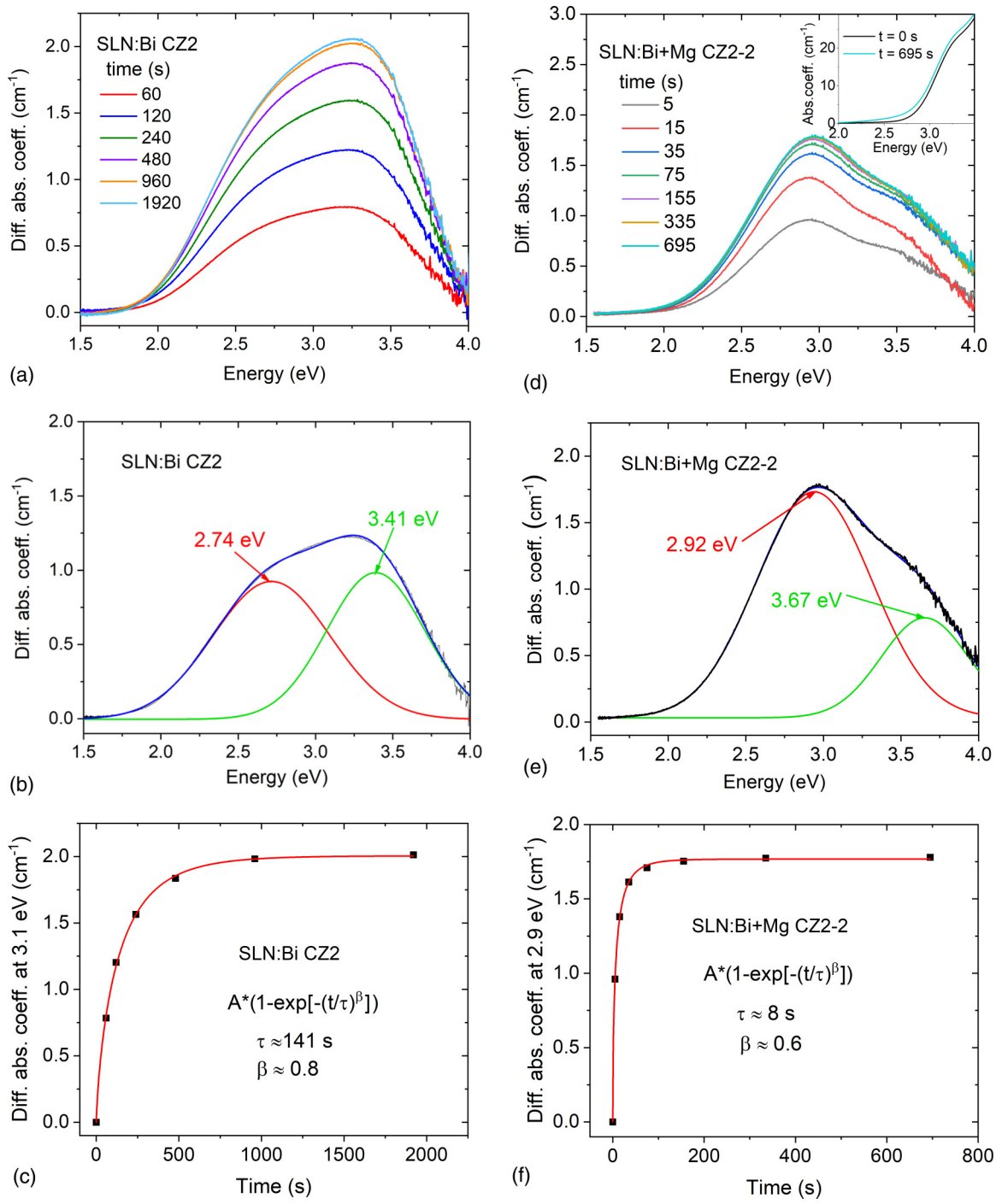

FIG. 6. Near-UV-induced absorption spectra for unpolarized light of Bi-doped (a) and (Bi,Mg)-codoped (d) crystals for increasing illumination time obtained by subtracting from each spectrum the one measured at $t = 0$ s shown in the double-doped case in the inset of (d) together with the spectrum at $t_{max} = 695$ s. Fits by two Gaussian components providing excellent reproductions of the spectra for both crystals (b,e). Buildup of the photochromic change at 3.1 eV in Bi-doped (c) and at 2.9 eV in (Bi,Mg)-codoped (f) SLN. Black dots: experimental data; red lines: stretched exponential fits with the parameters indicated.

oxygen with the concomitant transformation of Bi^{5+} to Bi^{3+}; this can be understood as the formation of $Bi_{Nb}^{2-} - V_O^{2+}$ defects (V_O^{2+} denoting an oxygen vacancy) where a lone pair essentially *replaces* an O^{2-} ligand. In LN, however, oxygen loss from the bulk, jointly with Li loss, may occur only during vacuum reduction above 650 °C [16]. The compound $KBiO_3$ [39] has a different cubic close-packed $KSbO_3$ structure due to the large K^+ ion known also for its role in the HTTSSG growth of SLN, where it only promotes the incorporation of smaller Li^+ ions.

In summary, the low-stability Bi^{5+} oxidation state only appears in the presence of additional alkali ions and prefers higher-symmetry coordination. In LN such octahedral sites are readily available; still the majority of Bi defects are

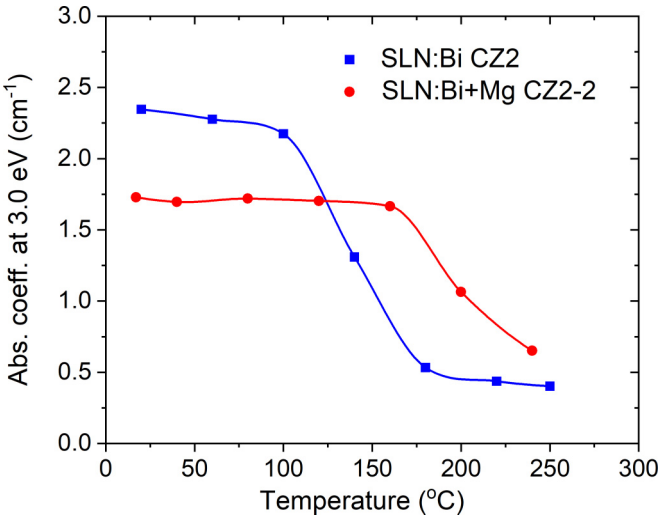

FIG. 7. Decay of near-UV-induced absorption measured as a function of temperature for SLN:Bi and SLN:(Bi,Mg) crystals. Lines are only guides for the eye.

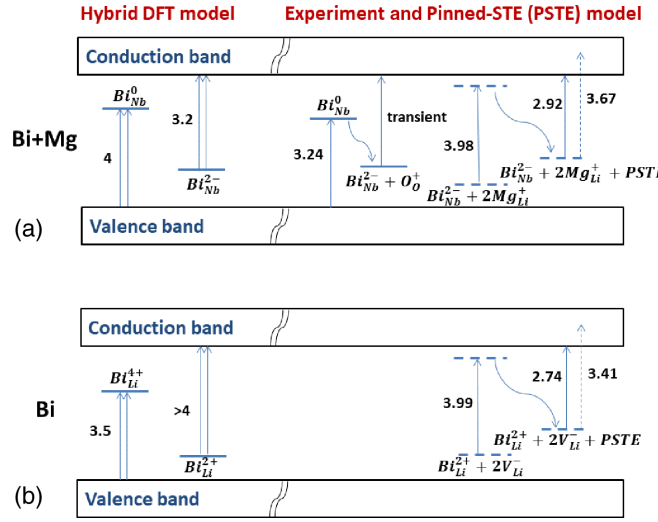

FIG. 8. Gap levels and absorption transitions in eV units of Bi defects in LN:(Bi,Mg) (a) and LN:Bi (b) according to the hybrid DFT model calculated in Refs. [7,8] (left) and our experiments in stoichiometric crystals interpreted by the pinned self-trapped exciton (PSTE) model (right). The dashed levels indicate the involvement of localized band states.

expected to be trivalent, losing symmetry and conserving local neutrality due to flexible charge-compensation mechanisms [16]. This is provided by lithium vacancies and protons having motional activation energies of only 1.29 eV [40] and ≈1.2 eV [41], respectively, presumably playing roles in the months-long recombination processes observed.

B. Gap states of $Bi^{5+/3+}$ and absorption bands in as-grown doped LN

Due to its larger electronegativity Bi^{5+} should have a gap level, empty in oxidized LN, below the conduction band formed of Nb states, and a slightly deeper one if incorporated on a larger Li site (with due charge compensation), as suggested by the comparison of Nb^{4+} levels of normal and antisite niobium [42]. Hybrid density functional theory calculations in the Li_2O-deficient limit [7,8] confirm these expectations, and suggest that, due to local lattice relaxation and lone-pair effects, also Bi^{3+} ions having a dominantly $6s^2$ configuration in LN (in contrast to $6p^2$ in low-symmetry oxides) may have even deeper, normally filled gap states. The Bi^{3+} charge state can also be considered as a one-site bipolaron in LN and brings to mind $Nb^{3+}_{Li} - Nb^{-}_{Nb}$ two-site bipolarons representing a deep gap state [42].

For Bi^0_{Nb}, the simplest case of Bi^{5+} requiring no charge compensation, Ref. [7] predicts a peak ≈3.45 eV above the valence band maximum with a corresponding absorption band at ≈4.0 eV due to filling of this gap state in a *valence band to gap state* transition [see Fig. 8(a)]. For the somewhat unrealistic case of Bi^{2-}_{Nb} without charge compensation, the gap state is assumed to be filled by the lone pair, but for the same reason predicted to be lowered by ≈2 eV (polaron and lone-pair effect); this leads to a ≈3.2 eV band due to a *gap state to conduction band* transition [7]. For the even less realistic case of Bi^{4+}_{Li} without charge compensation an empty $6s$ gap level is calculated yielding an absorption band at only 3.5 eV [see Fig. 8(b)]. As an attempt to account for partial charge compensation in a $Bi^{4+}_{Li} - V^{-}_{Li}$ complex, this level is calculated to be lowered by a few tenths of an eV. The gap levels should be further depressed in all cases if additional charge compensators are taken into account [8]. For Bi^{2+}_{Li}, the gap state, assumed to be filled, is again shifted deep to the bottom of the gap, thus enabling only absorption veiled by band to band transitions [7]. However, all these results may be influenced by unaccounted effects like multiparticle (configurational) interactions and the alkali-rich environments applied.

Therefore it is not surprising that the band energies obtained in [7,8] cause some difficulties when compared with our experimental results in closely stoichiometric crystals. Starting with SLN:(Bi,Mg) we indeed find two bands with different HWHMs and polarizations. Reference [7] attributes a ≈4.0 eV band (found by us to be intense, broad, and of nearly ordinary polarization) to the neutral Bi^0_{Nb} defect, and a band at ≈3.2 eV (found small, narrow, and of more extraordinary type) to Bi^{2-}_{Nb} defects, the latter in addition expected to cause inhomogeneous broadening due to various nearby charge compensators. In SLN:Bi the gap levels for both charge states are predicted to be lowered in different ways if realistic charge compensation is taken into account, while we only find a single band at ≈4.0 eV.

Part of the solution of the problem in SLN:(Bi,Mg) may be stable associations of the Bi defects with other defects mostly conserving or establishing neutrality, a tendency corroborated by [8]. For Bi^0_{Nb} a possible partner may be a neutral $Mg^+_{Li} - V^-_{Li}$ pair, and for Bi^{2-}_{Nb} defects simple charge compensators like Mg^+_{Li} or protons [for simple examples with Mg, see Figs. 9(c) and 9(d)]. In all cases association lowers the respective gap state energy resulting in opposite shifts of the absorption bands by several tenths of an eV; indeed, the direction of the band shift differs for cases involving transitions to and from the gap state. Neglected multiparticle interaction effects may also influence the band positions in opposite directions. So the bands may change places, accordingly, we propose *switched*

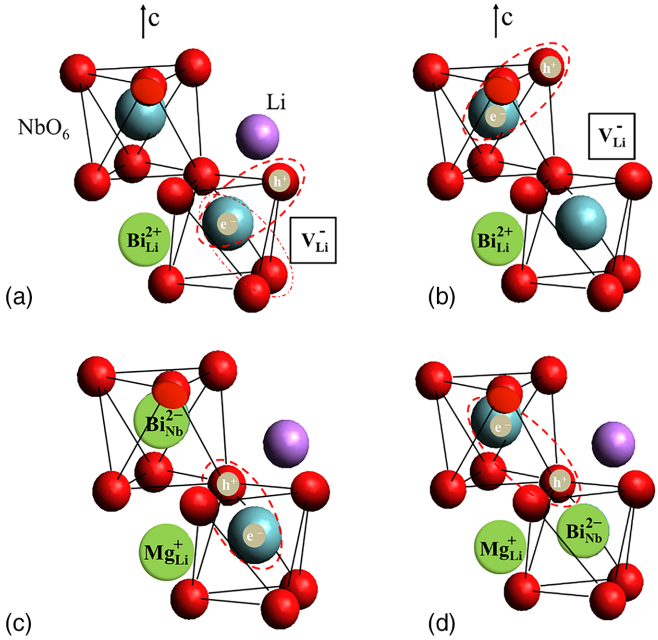

FIG. 9. Ionic models for dipolar $Bi_{Li}^{2+} - V_{Li}^{-}$ (a), (b) and $Bi_{Nb}^{2-} - Mg_{Li}^{+}$ (c), (d) defects and suggested positions of STEs (see dashed/dotted ellipses) pinned to them. Additional charge compensators at other nearby Li sites are not shown. Blue, purple, red, and green balls represent niobium, lithium, oxygen, and dopant atoms, respectively.

assignations: the narrow band at ≈3.24 eV characterized by $\theta = 36°$ should be attributed to neutral $Bi_{Nb}^{0}(-Mg_{Li}^{+} - V_{Li}^{-})$ type complexes, and the larger band at ≈4.0 eV with $\theta = 53°$, to various charge-compensated $Bi_{Nb}^{2-} - 2Mg_{Li}^{+}$ type defects. The problem in SLN:Bi apparently has similar reasons, preventing the separation of the different Bi_{Li} defects. This also means that the gap state in SLN:Bi is normally very deep and filled; this identifies the Bi_{Li}^{2+} charge state as the dominant ground state in SLN:Bi. From this analysis it is also clear that some of the clustered and charge-compensated Bi_{Li}^{2+} or Bi_{Nb}^{2-} defects may have very deep levels merging with the valence band and, for this reason, remain silent in absorption, explaining the absorption deficit in K-flux-grown crystals of high stoichiometry.

C. Excitations next to deep gap states leading to long-lived pinned STEs

More problematic is the slow buildup and the months-long persistence of near-UV-induced changes. As the great majority of defects in as-grown crystals are expected to be neutral, the excited Bi defects produced by ionizing processes should be short-lived doubly charged defects, taking into account the instability of Bi^{4+} ions. Such processes may indeed explain the laser-pulse-induced fast photorefractive response, but leave the long-lived photochromism unanswered. However, this controversy can be resolved by taking into account two circumstances: (i) due to the exchange interaction stabilizing the lone pair, a singly excited state may be qualitatively different from a doubly excited one and involve important admixtures of band states; (ii) with the exception of the neutral Bi_{Nb}^{0} defect the involved gap states are well within ≈1 eV of the valence band maximum. This signifies that instead of (or along with) charge transfers from Bi^{3+} to the Nb sublattice, for one-photon processes the transfers may essentially go from the oxygen ligands to nearby Nb ions, conserving the lone pair.

The iron *C* band [32,33], now clearly separated at 4.0 eV in SLN:Fe(<0.1 mol %) [Fig. 3(e)], and recently reinterpreted clarifying the role of charge compensators [14], shows close similarity to the Bi-related bands at 4 eV. Pulse-induced transient absorption measurements in CLN:Fe revealed a two-step process attributed to $Fe_{Li}^{2+} - nV_{Li}^{-}$ dipoles ($n = 2$ for most Fe^{3+} defects). First the buildup of a $Fe_{Li}^{2+} - Nb_{Nb}^{-} - O_{O}^{+} - nV_{Li}^{-}$ pinned STE was observed, either with $\tau_{buildup} \approx 5\ \mu s$ (for $E_{exc} = 4.66\ eV \geqslant E_{gap}$ required for formation + hopping transport + trapping of a free STE [13]), or quasi-instantaneously (for $E_{exc} = 3.49\ eV < E_{gap}$ only sufficient for local pinned-STE generation [14,15]). This was followed by spontaneous transformation into a $Fe_{Li}^{+} - O_{O}^{+} - nV_{Li}^{-}$ variant, still considered as a pinned exciton polaron, which had a longer lifetime of a few seconds at RT (monitored via the induced absorption band near 2.9 eV) until recombination lead to the recovery of the original defect [14,15]. While such a process as a whole corresponds to a reversible local electron transfer from an O^{2-} ion to an adjacent Fe^{3+} ion, no charge is released, since the electron is withheld by the adjacent temporarily existing trapped hole center. However, if repeatedly excited during its lifetime near or above 2.9 eV, ionization still may take place, similarly to the case of the ≈2.6 eV iron *D* band of more stable Fe^{2+} centers (mostly $Fe_{Li}^{+} - V_{Li}^{-}$ dipoles) [32,33]. A stable band at 4.03 eV discerned in CLN:Mg(6.5 mol %) at 3.8 K, first related to trapped-hole formation near Mg_{Nb} complexes [11], was also attributed to pinned-STE formation at the same defects [14]. Note that pinning reduces the energy of STEs; compared to the 4.7 eV excitation band maximum of STE luminescence [43], the 4 eV absorption band maximum arising upon Fe doping then indicates a 0.7 eV energy gain due to STE generation next to the defect dipole.

Based on the similar positions, polarizations and half widths of Fe- and Bi-related bands near 4.0 eV observed despite the radically different $3d^5$ and $6s^2$ electronic configurations of the involved dopant ions, we propose a similar interpretation also for the Bi case: generation of an adjacent Nb^{4+}–O^{-} group and no charge transfer involving the dopant itself. In SLN:Bi we accordingly assume $V_{Li}^{-} - Bi_{Li}^{2+} - V_{Li}^{-}$ defects to transform into $V_{Li}^{-} - Bi_{Li}^{2+} - Nb_{Nb}^{-} - O_{O}^{+} - V_{Li}^{-}$ type pinned-STE complexes which undergo substantial relaxation making them long lived. Their lifetime strongly depends on the positions of the charge compensators. Lithium vacancies may be preferably situated at second-nearest positions to Bi_{Li} [8] with the STE mainly localized on a Nb-O short bond between the Bi_{Li}^{2+} ion and a V_{Li}^{-} as shown by a dashed ellipse in Fig. 9(a). An additional dotted ellipse indicates that the relaxed defect may involve the other common oxygen neighbor of Nb_{Nb}^{-} and V_{Li}^{-} as well. The stability of the chain is warranted by attractive forces in all of its links: Bi_{Li}^{2+} obtains a closer charge-compensating Nb_{Nb}^{-} neighbor and the other end corresponds to an O^{-} trapped-hole center, stable up to RT [16]. Pinning in other, e.g., nearest-neighbor geometries

[Fig. 9(b)] also represents a bound state closely uniting the dipolar defect with the dipolar STE preventing recombination. Such attractive forces may prevent recombination up to the observed decay temperature of ≈ 180 °C in SLN:Bi. In SLN:(Bi,Mg), similarly, metastable pinned-excitonic $Mg_{Li}^{+} - Bi_{Nb}^{2-} - O_{O}^{+} - Nb_{Nb}^{-} - Mg_{Li}^{+}$ complexes stable up to ≈ 250 °C may be formed; for possible geometries see Figs. 9(c) and 9(d). Note that Mg_{Li}^{+} defects were discussed as stabilizers for Nb_{Nb}^{-} polarons [44]. The comparison of STEs pinned on Fe and Bi is deferred to the next section.

The polarization of the 4.0 eV bands (see Table II) corresponds to the average polar angle 55° of Nb–O bond directions ($\theta_{short} = 62.1°$ and $\theta_{long} = 47.8°$ for the short (1.88 Å) and long (2.13 Å) bond, respectively [45]). The HWHMs of 0.36 and 0.43 eV of these bands in variously doped SLN crystals are slightly larger than the HWHM of ≈0.3 eV of the excitation band of STE luminescence [43] which can be attributed to various possible positions of charge compensators, especially in (Bi,Mg)-codoped crystals where clusters containing Bi_{Li} left over despite Mg codoping may also yield some contribution.

The outstanding properties of the 3.24 eV band in SLN:(Bi,Mg) can be explained by the much weaker coupling of Bi_{Nb}^{0} to both the band states and the phonon spectrum. A fully isolated Bi_{Nb}^{0} would show fully extraordinary polarization and would not lead to STE trapping. Optional associations with neutral Mg or other defects reducing symmetry may explain some deviation from axial symmetry, in particular, the intermediary polarization angle θ.

D. Near-UV-induced bands—further excitations of pinned STEs

The persistent near-UV-induced bands at 2.74, 2.92, 3.41 and 3.67 eV also bring to mind "long-lived" transients in CLN:Fe($\leqslant$0.1 mol %) and CLN:Mg($\geqslant$5 mol %) (Table II and [17]). The blueshifted UV edge in CLN:Mg also allowed, apart from a 2.65 eV component, the observation of a second one at 3.45 eV [11]. As for those examples, for the Bi case we again propose the interpretation based on the existence and further excitation of pinned STEs (Fig. 8).

The positions of these bands, in contrast to the case of the practically unchanged 4 eV as-grown band, show perceptible variations which can be attributed to the different electronic configurations of the dopants. Much more spectacular are the markedly different decay times of the near-UV-induced bands, a few seconds for Fe^{3+} and months for Bi^{3+}. The main aspect of the configurational difference may be the different availability of singly recharged excited states: there is a readily available $3d^6$ state of the Fe^{2+} ion, while for the Bi^{3+} dopant ion, which has a deep $6s^2$ type lone-pair ground state, excitation to any singly recharged excited atomic state would require much more energy. Apparently, the different admixtures of those states to the various multielectron energy levels of the pinned STEs may strongly modify the dynamic behavior. Due to such effects the lone pair determines the exorbitant lifetime and thermal stability of the UV-induced bands in the Bi case. For each dopant the situation is substantially influenced by the charge-compensation and lattice relaxation mechanisms realized.

The bandwidths, viz. the W^2/M values of the components (M and W are the peak position and HWHM of a given band, respectively), are also similar for the various dopants compiled in Table II. In the absence of inhomogeneous broadening the W^2/M parameter characterizes the local electron-phonon coupling. For small polarons in LN $W^2/M \geqslant 0.1$ eV [42,11], while for the ≈4 eV band in SLN:Bi and SLN:Fe, its value is only 0.032 eV, despite inhomogeneous broadening. A value near 0.02 eV characterizes the excitation band of STE luminescence [43], indicating a substantially reduced electron-phonon coupling for free STEs having an essentially dipolar electric moment but no net charge. Accordingly, $W^2/M \approx 0.074$ or 0.063 eV for the lower energy near-UV-induced component indicates mixed properties between small-polaronic charge transfer and excitonic transfer restricted to Nb–O bonds, while the other component exhibits more excitonic character. It is unclear whether the two components belong to the same or different defect types.

The assignations proposed ensure the nearly fixed intensity ratio between both near-UV-induced components observed during pinned-STE generation, while deviations from such uniformity might be due, e.g., to overlap with polaronic bands. The amplitude of the band at ≈4 eV in as-grown crystals should correspond to the actual number of defect centers available for pinning. The fact that this amplitude does not change appreciably upon UV irradiation then indicates that only a small portion of the potential pinning centers leads to persistent pinning. The much smaller (1%–5%) saturation amplitudes of the near-UV-induced bands and their stretched-exponential buildup indeed confirm the existence of a broad distribution of pinned-STE lifetimes due to the existence of different defect configurations [14]. The buildup time also depends on the presence of other recombination centers and is shortened in SLN:(Bi,Mg) [Fig. 6(f)] due to the absence of exciton sinks like Nb_{Li} complexes known for their nanosecond-scale luminescence at low temperatures [14].

E. Exciton-polaronic and polaronic channels of photorefraction

STEs pinned to various Bi^{3+} defects, with strongly varying lifetimes, contribute to photorefractive phenomena by the combined effect of their overlapping as-grown and near-UV-induced bands. Depending on the applied intensity and wavelength, these processes may be important for photon energies down to ≈3 eV. For all Bi defects, a second excitation may lead to fast recombination (see also the "transient" indicated in Fig. 8).

For intense near-UV laser excitation, along with intrinsic processes, two-photon detrapping of lone pairs becomes important. In under-threshold Bi-single-doped crystals the generated small polarons may redistribute between intrinsic traps or get retrapped at metastable Bi centers. With increasing Bi concentration and improved stoichiometry, the intrinsic trapping processes become gradually suppressed, resulting in faster response times. In highly Mg-doped LN, only a limited number of OH^{2-} type trapped-electron centers and efficient hole traps of $Mg_{Nb}^{3-} - nMg_{Li}^{+}$ type ($n \leqslant 3$) can be assumed [46]. In SLN:(Bi,Mg) and apparently also in CLN:(Bi,Mg), however, Bi_{Nb}^{0} type defects and freshly ionized Bi complexes become the dominant electron traps. This may result in a fast

photorefractive effect without optical damage. Thus an optimum stoichiometry with an appropriate Mg level, allowing for sufficient Bi incorporation with a minimum number of intrinsic defects, must be found.

V. CONCLUSIONS

The incorporation of Bi in LN is found to be strongly influenced by the presence of additional cations in the melt or the flux: surplus Li^+ and K^+ improve stoichiometry and thereby decrease the Bi incorporation coefficient; K^+ also promotes oxidation of Bi^{3+} to Bi^{5+}, and Mg^{2+} forces cations with larger valence from Li to Nb substitution sites. The various absorption bands observed in SLN:Bi and SLN:(Bi,Mg) are separated and assigned to specific Bi defect types and their gap states, together with the respective persistent photochromic bands generated by near-UV irradiation. While photorefractive experiments and hybrid-DFT electron structure calculations have only been interpreted in terms of relaxed Bi^{3+} and Bi^{5+} type centers, implying two-particle processes and charge separation, we consider one-photon excitations and the consequences of the stability of exchange-coupled lone pairs: instead of breaking up the lone pair, we assume the generation of long-lived STEs pinned to charge-compensated dipolar Bi^{3+} defects. Defect-unspecific energy near the gap energy, polarization along Nb–O bonds, and a relatively small bandwidth serve as proof for the exciton-polaronic character of the bands observed near 4 eV. Similar exciton-polaronic states have earlier been characterized in systems like CLN [19], CLN:Fe and CLN:Mg [13–15], or $KTa_{1-x}Nb_xO_3$ [18], and discussed in ferroelectric oxides in general [20]. A theoretical approach to compute STEs from first principles has been proposed recently [47].

Accordingly, the formation of long-lived pinned STEs can be modeled by charge transfer along a specific O–Nb bond singled out by the geometry of the adjacent pinning defect consisting of a Bi^{3+} ion and its adjacent charge compensator(s), details depending on the Mg concentration. While this transfer near 4 eV does not directly result in separated electrons and holes, an option for charge separation is given by further excitation via the photoinduced bands of pinned STEs. These consist of a pair of component bands in the 2.7–3.7 eV range persistent on the months scale, Mg codoping only causing a small blueshift and a slightly higher thermal stability up to $\approx 250\,^{\circ}C$. For the explanation of the enhanced photorefractive properties of (Bi,Mg)-double-doped LN crystals, the active role of neutral Bi^0_{Nb} defects, weakly coupled to the lattice, providing a narrow transition at 3.24 eV, and serving also as electron traps, is proposed. Optimizing growth procedures, stoichiometry, and doping may further improve the application potential of the system.

ACKNOWLEDGMENTS

The authors are grateful to Dr. Éva Tichy-Rács and Gyula Kálmán for sample preparation and Dr. László Péter for the EDAX measurements. This research was supported by the Ministry of Culture and Innovation of Hungary and the National Research, Development and Innovation Office within the Quantum Information National Laboratory of Hungary (Grant No. 2022-2.1.1-NL-2022-00004).

[1] *Photorefractive Materials and Their Applications 2*, edited by P. Günter and J.-P. Huignard (Springer Science + Business Media, Berlin, 2007).

[2] D. Zheng, Y. Kong, S. Liu, J. Yao, L. Zhang, S. Chen, and J. Xu, The photorefractive characteristics of bismuth-oxide doped lithium niobate crystals, AIP Adv. **5**, 017132 (2015).

[3] D. Zheng, Y. Kong, S. Liu, M. Chen, S. Chen, L. Zhang, R. Rupp, and J. Xu, The simultaneous enhancement of photorefraction and optical damage resistance in MgO and Bi_2O_3 co-doped $LiNbO_3$ crystals, Sci. Rep. **6**, 20308 (2016).

[4] D. Zheng, W. Wang, S. Wang, D. Qu, H. Liu, Y. Kong, S. Liu, S. Chen, R. Rupp, and J. Xu, Real-time dynamic holographic display realized by bismuth and magnesium co-doped lithium niobate, Appl. Phys. Lett. **114**, 241903 (2019).

[5] S. Wang, Y. Shan, W. Wang, D. Zheng, H. Liu, S. Liu, Y. Kong, and J. Xu, Lone-pair electron effect induced a rapid photorefractive response in site-controlled $LiNbO_3$:Bi,*M* (*M* = Zn, In, Zr) crystals, Appl. Phys. Lett. **118**, 191902 (2021).

[6] S. Wang, Y. Shan, D. Zheng, S. Liu, F. Bo, H. Liu, Y. Kong, and J. Xu, The real-time dynamic holographic display of LN:Bi,Mg crystals and defect-related electron mobility, Opto-Electron. Adv. **5**, 210135 (2022).

[7] L. Li, Y. Li, and X. Zhao, Hybrid density functional theory insight into the stability and microscopic properties of Bi-doped $LiNbO_3$: Lone electron pair effect, Phys. Rev. B **96**, 115118 (2017).

[8] L. Li, Y. Li, and X. Zhao, Interaction between Bi dopants and intrinsic defects in $LiNbO_3$ from local and hybrid density functional theory calculations: Lone electron pair effect, Inorg. Chem. **58**, 3661 (2019).

[9] P. Herth, D. Schaniel, T. Woike, T. Granzow, M. Imlau, and E. Krätzig, Polarons generated by laser pulses in doped $LiNbO_3$, Phys. Rev. B **71**, 125128 (2005).

[10] D. Conradi, C. Merschjann, B. Schoke, M. Imlau, G. Corradi, and K. Polgár, Influence of Mg doping on the behaviour of polaronic light-induced absorption in $LiNbO_3$, Phys. Status Solidi RRL **2**, 284 (2008).

[11] F. Xin, Z. Zhai, X. Wang, Y. Kong, J. Xu, and G. Zhang, Threshold behavior of the Einstein oscillator, electron–phonon interaction, band-edge absorption, and small hole polarons in $LiNbO_3$:Mg crystals, Phys. Rev. B **86**, 165132 (2012).

[12] T. Kämpfe, A. Haußmann, L. M. Eng, P. Reichenbach, A. Thiessen, T. Woike, and R. Steudtner, Time-resolved photoluminescence spectroscopy of Nb^{4+} Nb and O^- polarons in $LiNbO_3$ single crystals, Phys. Rev. B **93**, 174116 (2016).

[13] S. Messerschmidt, A. Krampf, F. Freytag, M. Imlau, L. Vittadello, M. Bazzan, and G. Corradi, The role of self-trapped excitons in polaronic recombination processes in lithium niobate, J. Phys.: Condens. Matter **31**, 065701 (2019).

[14] G. Corradi, A. Krampf, S. Messerschmidt, L. Vittadello, and M. Imlau, Excitonic hopping-pinning scenarios in lithium niobate based on atomistic models: Different kinds of stretched

exponential kinetics in the same system, J. Phys.: Condens. Matter **32**, 413005 (2020).
[15] S. Messerschmidt, B. Bourdon, D. Brinkmann, A. Krampf, L. Vittadello, and M. Imlau, Pulse-induced transient blue absorption related with long-lived excitonic states in iron-doped lithium niobate, Opt. Mater. Express **9**, 2748 (2019).
[16] G. Corradi and L. Kovács, 'Horror vacui' in the oxygen sublattice of lithium niobate made affordable by cationic flexibility, Crystals **11**, 764 (2021).
[17] T. Volk, N. Rubinina, and M. Wöhlecke, Optical-damage-resistant impurities in lithium niobate, J. Opt. Soc. Am. B **11**, 1681 (1994).
[18] R. V. Yusupov, I. N. Gracheva, A. A. Rodionov, P. P. Syrnikov, A. I. Gubaev, A. Dejneka, L. Jastrabik, V. A. Trepakov, and M. K. Salakhov, Experimental manifestations of the $Nb^{4+} - O^{-}$ polaronic excitons in $KTa_{0.988}Nb_{0.012}O_3$, Phys. Rev. B **84**, 174118 (2011).
[19] F. Schmidt, A. L. Kozub, U. Gerstmann, W. G. Schmidt, and A. Schindlmayr, A density-functional theory study of hole and defect-bound exciton polarons in lithium niobate, Crystals **12**, 1586 (2022).
[20] V. S. Vikhnin, R. I. Eglitis, S. E. Kapphan, G. Borstel, and E. A. Kotomin, Polaronic-type excitons in ferroelectric oxides: Microscopic calculations and experimental manifestation, Phys. Rev. B **65**, 104304 (2002).
[21] K. Polgár, Á. Péter, L. Kovács, G. Corradi, and Zs. Szaller, Growth of stoichiometric $LiNbO_3$ single crystals by top seeded solution growth method, J. Cryst. Growth **177**, 211 (1997).
[22] M. Lee, S. Takekawa, Y. Furukawa, Y. Uchida, K. Kitamura, H. Hatano, and S. Tanaka, Photochromic effect in near-stoichiometric $LiNbO_3$ and two-color holographic recording, J. Appl. Phys. **88**, 4476 (2000).
[23] M. Lee, I. G. Kim, S. Takekawa, Y. Furukawa, Y. Uchida, K. Kitamura, and H. Hatano, Electron paramagnetic resonance investigation of the photochromic effect in near-stoichiometric $LiNbO_3$ with applications to holographic storage, J. Appl. Phys. **89**, 5311 (2001).
[24] L. Bencs, K. György, M. Kardos, J. Osán, B. Alföldy, I. Varga, N. Szoboszlai, Zs. Ajtony, Zs. Stefánka, É. Széles, and L. Kovács, Determination of trace elements in lithium niobate crystals by solid sampling and solution-based spectrometry methods, Anal. Chim. Acta **726**, 1 (2012).
[25] G. Dravecz, N. Laczai, I. Hajdara, and L. Bencs, Solid sampling determination of magnesium in lithium niobate crystals by graphite furnace atomic absorption spectrometry, Spectrochim. Acta, Part B **126**, 1 (2016).
[26] K. Nassau, Lithium niobate—a new type of ferroelectric: Growth, structure, and properties, in *Ferroelectricity, Proceedings of a Symposium*, edited by E. F. Weller (Elsevier, Amsterdam, 1967).
[27] R. D. Shannon, Revised effective ionic radii and systematic studies of interatomic distances in halides and chalcogenides, Acta Crystallogr., Sect. A **32**, 751 (1976).
[28] G. Dravecz and L. Kovács, Determination of the crystal composition from the OH^{-} vibrational spectrum in lithium niobate, Appl. Phys. B **88**, 305 (2007).
[29] Á. Péter, K. Polgár, L. Kovács, and K. Lengyel, Threshold concentration of MgO in near-stoichiometric $LiNbO_3$ crystals, J. Cryst. Growth **284**, 149 (2005).
[30] L. Kovács, L. Kocsor, É. Tichy-Rács, K. Lengyel, L. Bencs, and G. Corradi, Hydroxyl ions probing transition metal dopants occupying Nb sites in stoichiometric $LiNbO_3$, Opt. Mater. Express **9**, 4506 (2019).
[31] M. Wöhlecke and L. Kovács, OH^{-} ions in oxide crystals, Crit. Rev. Solid State Mater. Sci. **26**, 1 (2001).
[32] M. G. Clark, F. J. DiSalvo, A. M. Glass, and G. E. Peterson, Electronic structure and optical index damage of iron-doped lithium niobate, J. Chem. Phys. **59**, 6209 (1973).
[33] B. Dischler, J. R. Herrington, A. Räuber, and H. Kurz, Correlation of the photorefractive sensitivity in doped $LiNbO_3$ with chemically induced changes in the optical absorption spectra, Solid State Commun. **14**, 1233 (1974).
[34] K. H. Whitmire, Bismuth: Inorganic chemistry, in *Encyclopedia of Inorganic and Bioinorganic Chemistry*, edited by R. A. Scott (Wiley, New York, 2013).
[35] S. A. Ivanov, R. Tellgren, H. Rundlof, and V. G. Orlov, Structural studies of Bi_2O_3 by neutron powder diffraction, Powder Diffr. **16**, 227 (2001).
[36] N. Kumada, N. Kinomura, P. M. Woodward, and A. W. Sleight, Crystal structure of Bi_2O_4 with β-Sb_2O_4-type structure, J. Solid State Chem. **116**, 281 (1995).
[37] N. Kumada, N. Takahashi, N. Kinomura, and A. W. Sleight, Preparation and crystal structure of a new lithium bismuth oxide: $LiBiO_3$, J. Solid State Chem. **126**, 121 (1996).
[38] N. Kumada, N. Kinomura, and A. W. Sleight, Neutron powder diffraction refinement of ilmenite-type bismuth oxides: $ABiO_3$ (A = Na, Ag), Mater. Res. Bull. **35**, 2397 (2000).
[39] S. Kodialam, V. C. Korthius, R.-D. Hoffmann, and A. W. Sleight, Electrodeposition of potassium bismuthate: $KBiO_3$, Mater. Res. Bull. **27**, 1379 (1992).
[40] A. Krampf, M. Imlau, Y. Suhak, H. Fritze, and S. Sanna, Evaluation of similarities and differences of $LiTaO_3$ and $LiNbO_3$ based on high-T-conductivity, nonlinear optical fs-spectroscopy and *ab initio* modeling of polaronic structures, New J. Phys. **23**, 033016 (2021).
[41] L. Dörrer, P. Tuchel, E. Hüger, R. Heller, and H. Schmidt, Hydrogen diffusion in proton-exchanged lithium niobate single crystals, J. Appl. Phys. **129**, 135105 (2021).
[42] O. F. Schirmer, M. Imlau, C. Merschjann, and B. Schoke, Electron small polarons and bipolarons in $LiNbO_3$, J. Phys.: Condens. Matter **21**, 123201 (2009).
[43] D. M. Krol, G. Blasse, and R. C. Powell, The influence of the Li/Nb ratio on the luminescence properties of $LiNbO_3$, J. Chem. Phys. **73**, 163 (1980).
[44] V. G. Grachev and G. I. Malovichko, Structures of impurity defects in lithium niobate and tantalate derived from electron paramagnetic and electron nuclear double resonance data, Crystals **11**, 339 (2021).
[45] S. C. Abrahams and P. Marsh, Defect structure dependence on composition in lithium niobate, Acta Crystallogr., Sect. B **42**, 61 (1986).
[46] I. M. Zaritskii, L. G. Rakitina, G. Corradi, K. Polgár, and A. A. Bugai, A new trapped-hole radiation defect in heavily Mg-doped $LiNbO_3$, J. Phys.: Condens. Matter **3**, 8457 (1991).
[47] Z. Dai, C. Lian, J. Lafuente-Bartolome, and F. Giustino, Excitonic polarons and self-trapped excitons from first-principles exciton-phonon couplings, Phys. Rev. Lett. **132**, 036902 (2024).